ACS OMEGA

Open Access

http://pubs.acs.org/journal/acsodf

Article

Visible Light Induced Photocatalytic Degradation of Diclofenac in Aqueous Solution Using Fabricated ZnO/g-C_3N_4 by Facile Calcination Technique

Mahmudul Hassan Suhag,* Aklima Khatun, Ikki Tateishi, Mai Furukawa, Hideyuki Katsumata, and Satoshi Kaneco*

Cite This: *ACS Omega* 2024, 9, 45090−45103

Read Online

ACCESS | Metrics & More | Article Recommendations | Supporting Information

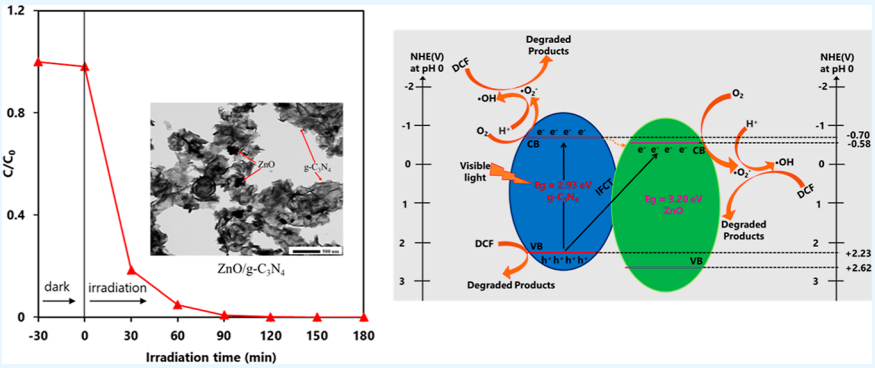

ABSTRACT: The ability of the heterojunction between two distinct semiconductors with appropriately matched band gaps to improve the separation of photogenerated electron−hole pairs has been demonstrated to enhance photocatalytic activity. Hence, ZnO/g-C_3N_4 composites have been fabricated by the facile deposition and calcination of ZnO and g-C_3N_4. X-ray photoelectron spectroscopy, powder X-ray diffraction, and Fourier transform infrared spectroscopy confirm the formation of the composite. Scanning electron microscope, transmission electron microscope, and energy-dispersive X-ray spectroscopy morphological analysis reveal that ZnO was homogeneously spread over the g-C_3N_4 surface. UV−vis diffuse reflectance spectroscopy analysis shows the slightly enhanced visible light absorption ability of the composite. Photoluminescence (PL) spectroscopy and electrochemical impedance spectroscopy analysis prove the higher charge separation of the composite during the irradiation of light. The composite shows admirable photocatalytic efficiency in the visible light-driven photocatalytic degradation of an aqueous diclofenac (DFC) solution. The superoxide anion radical ($\bullet O_2^-$) and hydroxyl radical (•OH) act as reactive species during the degradation reaction. Probable reaction mechanisms have been proposed.

INTRODUCTION

Pharmaceutical products and personal care items have been found in aquatic environments more frequently as a consequence of an enormous increase in utilization.[1] The synthetic nonsteroidal anti-inflammatory drug diclofenac (DCF), as its sodium salt, is most frequently applied in the treatment of inflammatory illnesses, dysmenorrhea for both humans and animals, and in personal care items.[2−4] The widely used DCF releases continuously into the aquatic environment through a variety of sources, including the metabolism of human and animal urine and feces after medical treatment, production site disposal, and domestic waste discharge.[1,5] Due to the low biodegradability and longtime environmental persistence of DCF, it is very frequently found in wastewater treatment plants, surface water, drinking water, groundwater, seawater, suspended soil, sediments, landfills, and sludge.[6,7] Furthermore, despite the fact that DCF concentrations in the environment have been reported to be numerous mg/L or ng/L, they may have negative impacts on ecosystems or human health.[8,9] For example, DFC impacts aquatic life, including rainbow and brown trout, by drastically mutating their gill cells, kidneys, and liver. Moreover, DFC is lethal to vultures while they consume the dead bodies of birds and animals treated with it.[4,10] Therefore, there is an urgent need to develop efficient techniques for removing DCF from wastewater and effluents. However, the DCF is not fully removed by conventional techniques such as adsorption, oxidation,

Received: June 18, 2024
Revised: August 1, 2024
Accepted: August 13, 2024
Published: October 30, 2024

coagulation, membrane, and electrochemical methods.[11−15] Advanced oxidation processes, including ozonation, UV/H_2O_2, sonolysis, and Fenton and photo-Fenton, have been used as promising methods to accomplish efficient removal of DCF as it is entirely mineralized.[2,16−22] Among these technologies, visible light-responsive semiconductor base photocatalytic degradation of DCF is regarded as an effective technique due to the high efficacy, cost-effectiveness, and potential utilization of solar energy.[7,23] This technique is based on the generation of electron−hole pairs, hydroxyl radicals, and superoxide radicals upon irradiation of light on the photocatalysts. All of the above-mentioned reactive species have the ability to attack organic contaminants, break them up into smaller pieces, and then mineralize carbon dioxide, water, and other inorganic species.[6] Numerous semiconductor- based photocatalysts have been utilized for the removal of DFC from water.[24]

The graphitic carbon nitride (g-C_3N_4) is widely used as a visible light-responsive photocatalyst owing to its appealing characteristics such as a narrow band gap (∼2.70 eV), good chemical stability, π-conjugated electronic structure, and suitable redox potential for the degradation of organic pollutants.[2,25] In addition, it is facile to fabricate g-C_3N_4 from several nitrogen-rich chemical substances, including dicyandiamide, urea, melamine, and thiourea, by thermally treating.[26] Nevertheless, the short lifetime of photogenerated charges due to the fast recombination of electron (e^-) and hole (h^+) pairs on pure g-C_3N_4 results in low photocatalytic activity of pure g-C_3N_4.[3] Moreover, a single-component photocatalyst with a broad range of light-absorption ability and good charge-separation efficacy is very challenging.[10] Hence, a large number of modified g-C_3N_4 by heterostructure formation with other semiconductors and doping with metals and nonmetals elements have been reported for the removal of DCF. For instance, Ag/g-C_3N_4, AgI/g-C_3N_4, V_2O_5/boron doped g-C_3N_4, Ti_3C_2/g-C_3N_4, TiO_2/g-C_3N_4, Co_3O_4/g-C_3N_4, and Ag_3PO_4/g-C_3N_4 composites have been utilized to degrade DCF as visible light-driven photocatalysts.[1−3,10,27−29]

ZnO is considered a well-known, cost-effective, and nontoxic photocatalytic semiconductor.[26] But it is inactive in the visible region and shows photocatalytic activity only in the ultraviolet region due to its higher band gap energy of about 3.2 eV.[30] However, the band level positions for ZnO and g-C_3N_4 match suitably. Hence, composites of g-C_3N_4 (medium band gap) and ZnO (wider band gap) may enhance the efficacy of photogenerated electron hole pair separation and transfer for the appropriate band position, resulting in enhanced photocatalytic activity.[31,32] Hence, the ZnO/g-C_3N_4 composite has attracted a lot of interest because of its excellent structure, dimensional anisotropy, optical, and electronic characteristics.[33] The ZnO/g-C_3N_4 composites have been fabricated in several research works using numerous techniques like calcination, ball milling, vapor condensation, reflux, ultrasonic dispersion, etc.[34−37]

In recent years, numerous research articles have been reported on the enhanced visible light-driven photocatalytic efficacy of ZnO/g-C_3N_4 composites for various applications such as generation of H_2, reduction of CO_2, inactivation of bacteria, degradation of dyes, removal of pharmaceutical products, and reduction of Cr(VI).[33,38−46] For instances, Meena et al. reported the synthesis of g-C_3N_4/ZnO nanostructures through mechano-thermal procedures for enhanced visible light-illuminated photocatalytic degradation of methylene blue dye.[47] Girish et al. prepared Z-scheme ZnO/g-C_3N_4 heterostructure using simply microwave irradiation as efficient visible light-driven photocatalysts for dye degradation and hydrogen evolution reactions.[48] Pham et al. reported the synthesis of ZnO/g-C_3N_4 composite by calcination technique and applied it to the solar light-assisted photodegradation of tetracycline in wastewater and the conversion of CO_2 as efficient photocatalyst.[49] Hosseini-Hosseinabad et al. reported the development of g-C_3N_4/ZnO nanocomposite as a highly effective photocatalytic and antibacterial novel cotton fabric coating.[50]

In the removal of pharmaceutical waste from aqueous effluent, the ZnO/g-C_3N_4 composites have been utilized to the degradation of sulfamethoxazole, nitenpyram, tetracycline, sulfonamides, endocrine disruptors, and more.[51−55] However, the photocatalytic degradation of DCF using ZnO/g-C_3N_4 composites has been rarely reported.

In this study, ZnO/g-C_3N_4 composites have been fabricated by the facile deposition and calcination of ZnO and g-C_3N_4. The visible light induced photocatalytic degradation of DCF using fabricated ZnO/g-C_3N_4 composites has been studied. Furthermore, the effects of the types of g-C_3N_4 and ZnO and the calcination temperature during composite formation have been inspected. The various parameters, including ZnO content in the composite, catalyst dosage, and initial concentration of DCF, have been optimized for visible light-driven photocatalytic DCF removal in aqueous solution. In addition, radical scavenger tests were also conducted to predict the degradation mechanism. The photocatalysts were also characterized utilizing different characterization methods.

MATERIALS AND METHODS

Materials. Diclofenac sodium (DCF, 98.0%), urea (99.0%), melamine (99.0%), zinc nitrate hexahydrate (99.9%), zinc acetate dihydrate (99.0%), ethanol (99.5%), isopropanol (IPA, 99.7%), benzoquinone (BQ, 98.0%), ethylenediaminetetraacetic acid (EDTA, 98.0%), nitric acid (61.0%), and sodium hydroxide (97.0%) were obtained from FUJIFILM Wako Pure Chemical Corporation, Japan. Two types of ZnO nanoparticles were purchased from Sigma-Aldrich (50−90 nm, 1−25 m^2 g^{-1}) and FUJIFILM WAKO Pure Chemical Corporation (∼5 μm). Formic acid (98.0%) and acetonitrile (99.5%) were obtained from Nacalai Tesque Inc. and Japan Kanto Chemical Co., Inc., Japan, respectively. All of the chemicals were analytical grade and used without more purification. An ultrapure water system (Advantec MFS Inc., Tokyo, Japan) was used for a pure water supply.

Synthesis of g-C_3N_4. Pure g-C_3N_4 was synthesized by the calcination of urea. Typically, 12 g of urea was ground manually, placed in a crucible, and covered by a cap and aluminum foil. Then it was calcined at 550 °C for 2 h with a heating increasing rate of 2 °C min^{-1} using an electric muffle furnace. Finally, the obtained light-yellow sample was grounded manually.

Preparation of ZnO/g-C_3N_4 Composite. A mixture of 150 mg of g-C_3N_4 and 50 mg of ZnO in 10 mL of ethanol was dispersed ultrasonically for 30 min, followed by stirring at a constant speed for 2 h. After that, the mixture was dried by centrifugation and vacuum oven. Finally, the dried mixture was calcined at 400 °C for 1 h with a heating increasing rate of 2 °C min^{-1} and ground in a mortar manually into a light-yellow powder. The schematic diagram of the fabrication of the ZnO/g-C_3N_4 composite is presented in Figure S1.

https://doi.org/10.1021/acsomega.4c05679
ACS Omega 2024, 9, 45090−45103

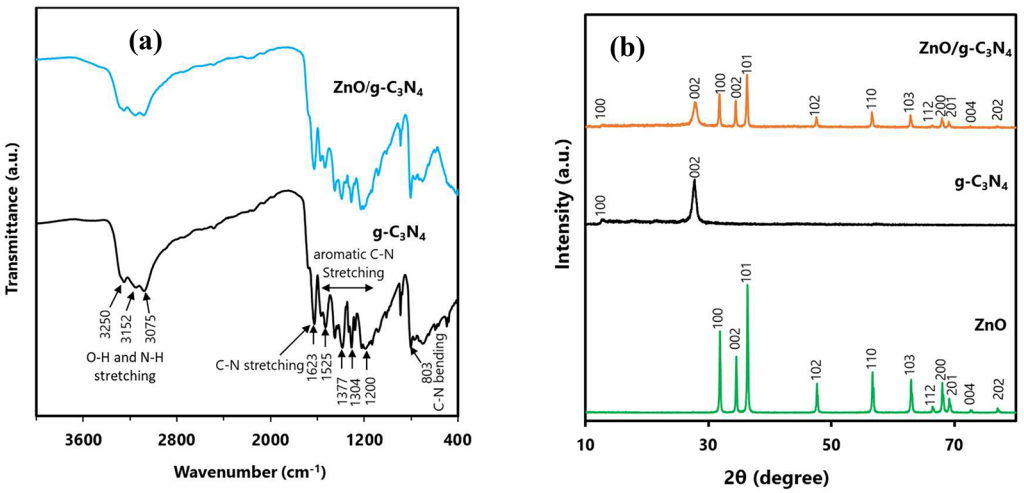

Figure 1. (a) FTIR spectra of g-C_3N_4 and ZnO/g-C_3N_4, and (b) XRD patterns of ZnO, g-C_3N_4, and ZnO/g-C_3N_4.

Characterization. The samples were characterized by X-ray diffraction (XRD), Fourier transform infrared (FTIR) spectroscopy, X-ray photoelectron spectroscopy (XPS), scanning electron microscope (SEM), energy-dispersive X-ray spectroscopy (EDS), transmitted electron microscope (TEM), UV−vis diffuse reflectance spectroscopy (DRS), PL spectroscopy, nitrogen adsorption and desorption isotherms, and electrochemical impedance spectroscopy (EIS) analysis. XRD patterns of the samples were attained by utilizing a Rigaku RINT Ultima-IV diffractometer by Cu Kα radiation in a scan range of 10−80° at a scan rate of 0.04°/s. The FTIR spectra of the photocatalysts were obtained by means of a PerkinElmer spectrometer (SPECTRUM 100 FTIR) with an attenuated total reflection assemblage. XPS of ZnO/g-C_3N_4 and g-C_3N_4 were characterized by using a PHI Quantera SXM photoelectron spectrometer with Al Kα radiation. SEM and EDS of the samples were investigated by using a JEOL JEM-1400 Flash SEM. The TEM of the samples was analyzed by means of a JEOL JEM-1011 TEM. The UV−vis DRS of the samples were inspected by a JASCO V-750 UV−vis instrument equipped by an integrating sphere adaptor. Photoluminescence (PL) spectra of the samples were attained with an excitation wavelength of 340 nm by utilizing a Shimadzu fluorescence spectrophotometer (RF-5300PC). The specific surface area, total pore volume, and average pore size of the photocatalysts were assessed from the N_2 adsorption−desorption isotherm utilizing a BELSORPminiII (MicrotracBE) instrument. The EIS and Mott−Schottky measurement of the photocatalysts was achieved on an electrochemical Versa STAT 3 workstation (Princeton Applied Research) equipped by a conventional three-electrode system. Here, a uniform slurry of the sample by Nafion solution was coated on a fluorine-doped tin oxide glass plate to make the working electrode, and an aqueous solution of Na_2SO_4 (0.5 mol L^{-1}) was utilized as the electrolyte. Pt wire and KCl-saturated AgCl/Ag were used as counter electrode and reference electrode, respectively.

Photocatalytic Degradation Experiment. The photocatalytic degradation of DCF by fabricated ZnO/g-C_3N_4 was investigated for 3 h with the irradiation of visible light at room temperature. A 50 mL pyrex glass cell was utilized for the photocatalytic degradation experiment. At optimal conditions, 30 mg of ZnO/g-C_3N_4 and 30 mL of aqueous solution of DCF (10 mg L^{-1}) were added to the glass cell and allowed for 30 min by magnetic stirring in the dark condition to establish adsorption−desorption equilibrium. Then, an LED lamp (OptoCode LDA14L-G/100W) with a UV (400 nm) cutoff filter (Y-44, HOYA) was placed on one side of the glass cell and used to expose the aqueous solution containing DCF and photocatalyst. Through the experiment, 1.5 mL of suspensions were collected at regular intervals of 30 min for analysis and centrifuged for 5 min at 10,000 rpm to isolate the photocatalyst. Then, the supernate was analyzed for the determination of the DCF concentration. A high-performance liquid chromatograph assembled with a separation column ODS-2 (GL Science Inc.) and a SHIMADZU UV/vis detector (UV 7750) was used to assess the quantity of DCF in the solution. The chromatogram was observed at wavelength of 276 nm. A mixture of acetonitrile and water (60:40, v/v) with 0.02% (v/v) of formic acid was used as mobile phase at isocratic mode. The flow rate of the mobile phase was 1.0 mL min^{-1}. The degradation experiment of DCF by other photocatalysts was also investigated under analogous photocatalytic experimental conditions. Moreover, the photolysis of DCF was also inspected under similar conditions. For establishing the optimal photocatalytic degradation condition of DCF by synthesized ZnO/g-C_3N_4, impact of variable operational conditions such as ZnO content in the composite (different ratio of used ZnO and g-C_3N_4), calcination condition of the fabrication of composite (different calcination temperature), types of ZnO and g-C_3N_4 in composite (sources of the precursors), dosage of catalyst (5 mg/30 mL to 50 mg/30 mL), and initial concentration of DCF (5 to 50 mg L^{-1}) were also inspected. To study the role of reactive species of •OH, h^+ and $•O_2^-$ for photocatalytic degradation of DCF with ZnO/g-C_3N_4, scavenger tests were carried out in the same optimal conditions utilizing IPA, EDTA and BQ as scavengers of the radical, respectively. The recyclability of the ZnO/g-C_3N_4 composite for photodegradation of DCF was inspected.

Moreover, the reaction rates as well as kinetics of the photocatalytic degradation procedure have been investigated according to the Langmuir−Hinshelwood (L−H) theory transformed by Turchi and Ollis. The theory was stated by eq 1.

$$r_0 = -\frac{dC}{dt} = \frac{kKC}{1 + KC} \quad (1)$$

https://doi.org/10.1021/acsomega.4c05679
ACS Omega 2024, 9, 45090−45103

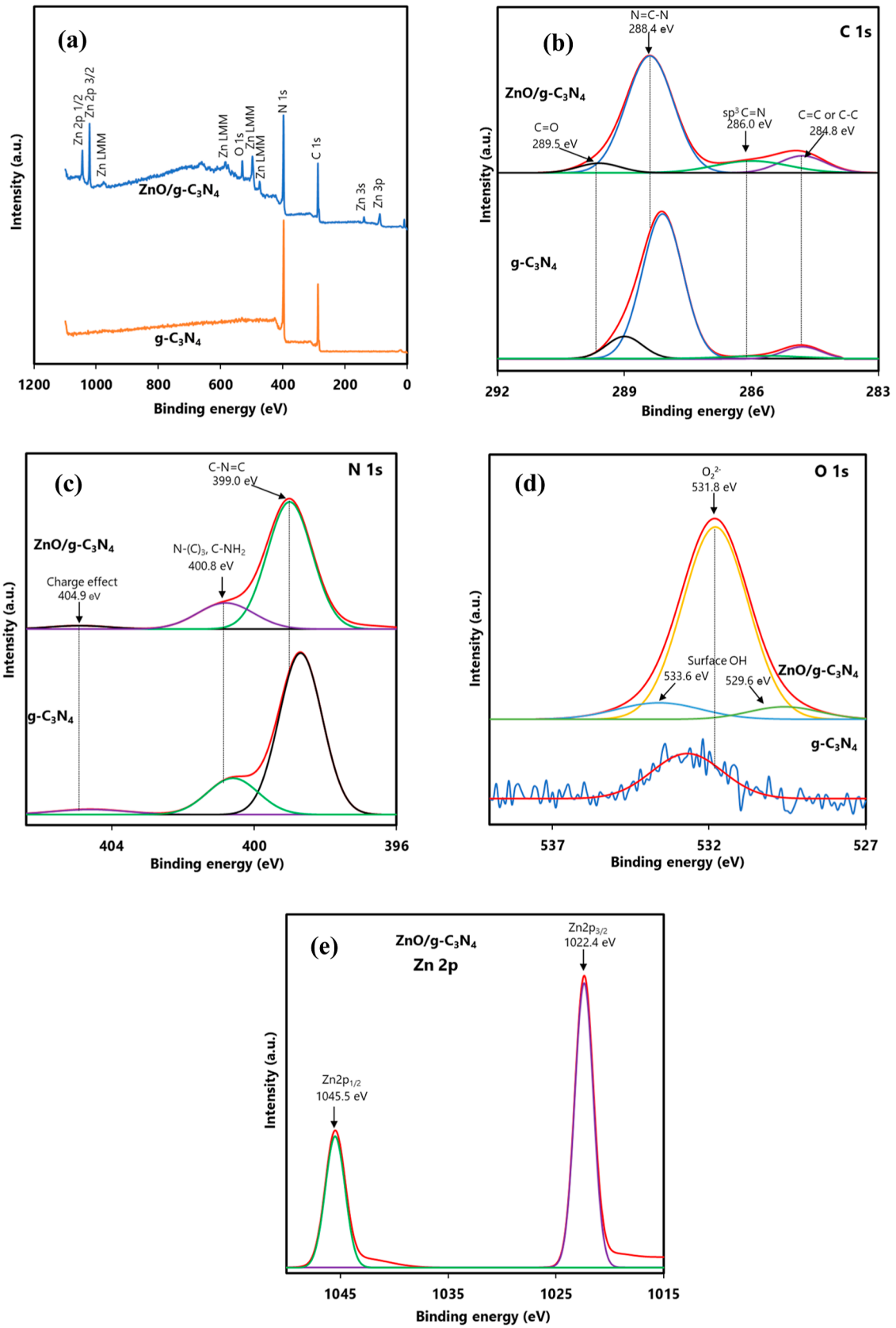

Figure 2. (a) Survey XPS spectra of g-C_3N_4 and ZnO/g-C_3N_4; overlap high resolution XPS (b) C 1s, (c) N 1s and (d) O 1s spectra of g-C_3N_4 and ZnO/g-C_3N_4 and (e) High resolution XPS Zn 2p spectra of ZnO/g-C_3N_4.

where r_0, k, C, and K are the degradation rate, the rate constant, reactant concentration, and adsorption equilibrium constant of the reaction, respectively. The eq 1 can be shortened to eq 2 if the initial concentration of C_0 is insignificant.

https://doi.org/10.1021/acsomega.4c05679
ACS Omega 2024, 9, 45090−45103

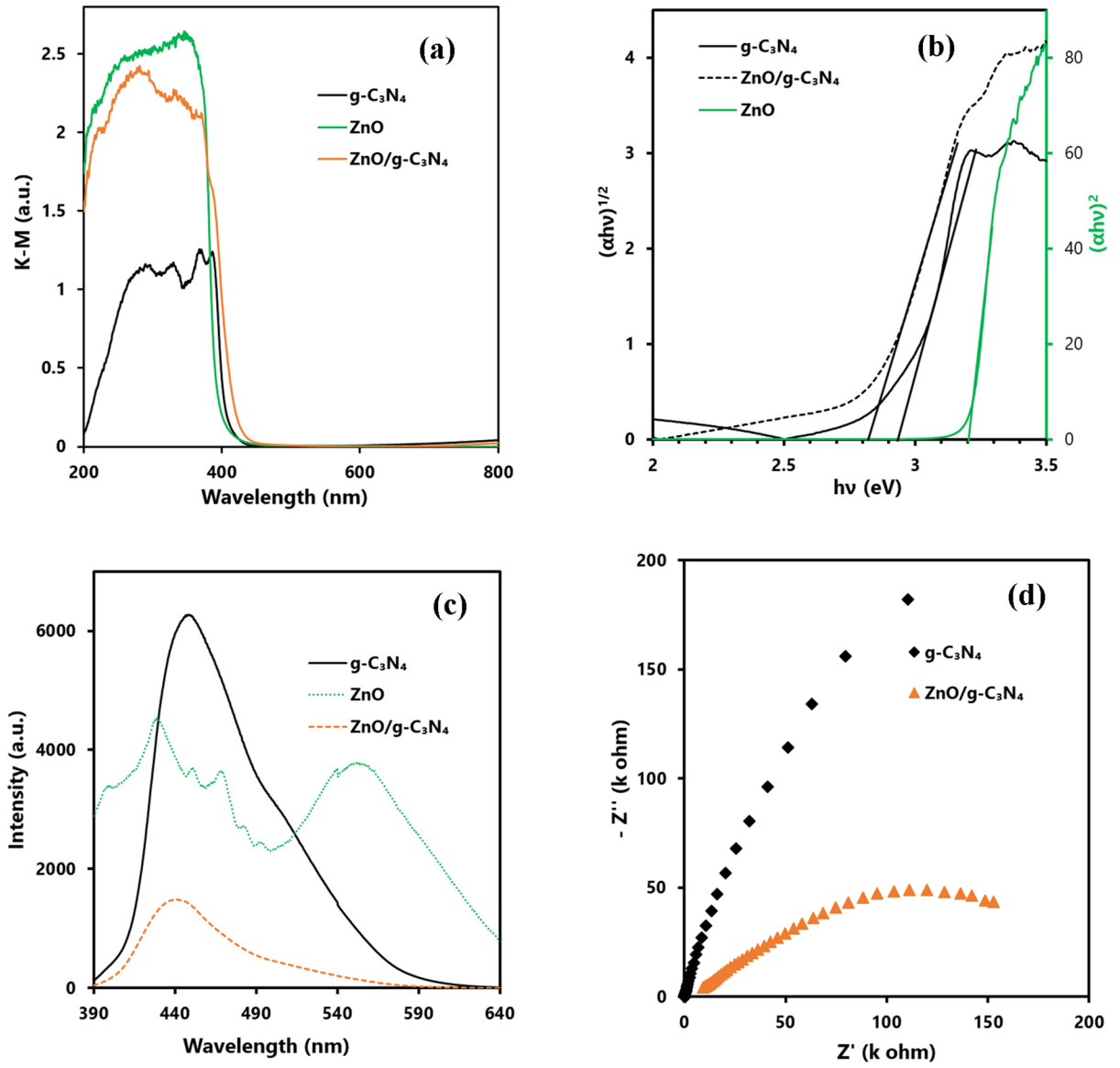

Figure 3. (a) Kubelka–Munk function of UV–vis DRS, (b) Tauc plot, and (c) PL spectra (upon the excitation at 340 nm wavelength) of ZnO, g-C_3N_4, and ZnO/g-C_3N_4, and (d) EIS resultant Nyquist plot of g-C_3N_4 and ZnO/g-C_3N_4.

$$-\ln\left(\frac{C}{C_0}\right) = kKt = k_{obs}t \quad (2)$$

With regard to the $-\ln(C/C_0)$, eq 2 forms a linear expression on time t, where k_{obs} is the reaction rate constant. The k_{obs} values in degradation reactions were determined by plotting $-\ln(C/C_0)$ versus time (t).

RESULTS AND DISCUSSION

FTIR Analysis. The fabrication of the ZnO/g-C_3N_4 composite was investigated by FTIR spectroscopy. The FTIR spectra of g-C_3N_4 and ZnO/g-C_3N_4 are shown in Figure 1a. Pure g-C_3N_4 revealed a peak at 1623 cm^{-1} attributed to the C–N stretching vibration mode and a number of peaks from 1200 to 1600 cm^{-1} assigned to aromatic C–N stretching. Furthermore, a peak was observed at 803 cm^{-1} corresponding to the out-of-plane stretching vibrational mode of the C–N heterocycle of the triazine ring.[56] A wide band of a few peaks with small intensity in the FTIR spectrum of g-C_3N_4 was observed between 2950 and 3300 cm^{-1} due to the O–H bond stretching vibration from the moisture or adsorbed water and deformed N–H stretching modes.[57] The FTIR spectra of ZnO/g-C_3N_4 showed similar peaks, like those of g-C_3N_4. Moreover, as shown in Figure S2, the positions of a few peaks corresponding to different C–N stretching and bending in the FTIR spectra of the ZnO/g-C_3N_4 were slightly shifted to the higher wavenumber compared to relevant peaks in the FTIR spectra of the pure g-C_3N_4, which indicated the interaction between ZnO and g-C_3N_4 in the ZnO/g-C_3N_4.[58]

XRD Analysis. Figure 1b shows the XRD patterns of ZnO, g-C_3N_4, and the ZnO/g-C_3N_4 composite. The diffraction peaks at 2θ values of 31.92, 34.64, 36.42, 47.68, 56.76, 63.14, 66.44, 67.98, 69.80, 72.92, and 77.28 were observed conforming to the plane of (100), (002), (101), (102), (110), (103), (200), (112), (201), (004), and (202), respectively, attributed to the structure of hexagonal wurtzite ZnO (JCPDS card no. 36-1451).[59,60] In addition, it can be seen from the XRD pattern of g-C_3N_4 that two distinct peaks were observed at 2θ values of 12.98 and 27.88, assigning them to the planes of (100) and

https://doi.org/10.1021/acsomega.4c05679
ACS Omega 2024, 9, 45090–45103

(002) corresponding to the repeating arrangement of the s-triazine unit and the conjugated aromatic system containing interplanar C−N stacking, respectively. The obtained XRD pattern shows that g-C_3N_4 is in its crystalline phase and that no secondary phases or contaminants are present (JCPDS card no. 87-1526).[52,61] As shown in the XRD pattern of ZnO/g-C_3N_4, both representative diffraction peaks of ZnO and g-C_3N_4 were detected, and no new extra peaks were noticed. Moreover, the positions of the corresponding characteristic peaks of ZnO and g-C_3N_4 remains unchanged. This demonstrates that two-phase compositions of g-C_3N_4 and ZnO were present in the prepared ZnO/g-C_3N_4, and there were no effects on the lattice structure of g-C_3N_4 and ZnO.[62]

XPS Analysis. Using the XPS survey spectrum, the surface elemental composition and their oxidation states of the g-C_3N_4 and ZnO/g-C_3N_4 composites were studied. As shown in Figure 2a, the fundamental-level binding energy peaks of C and N are clearly visible in both spectra. Moreover, for the spectra of ZnO/g-C_3N_4, characteristic peaks that corresponded to the binding energy values of Zn and O were appeared. The results suggested the formation and purity of the ZnO/g-C_3N_4 composite.[32] As shown in Figure 2b, the high-resolution C 1s XPS spectra of ZnO/g-C_3N_4 can be deconvoluted into four peaks at 284.8, 286.0, 288.4, and 289.5 eV, which are ascribed to the C═C or C−C bond, sp^3 C−N bond, s-triazine ring containing N═C−N groups, and C−O groups carried by the inevitable oxidation of the sample, respectively.[63] As shown in Figure 2c, the high-resolution N 1s XPS spectrum of ZnO/g-C_3N_4 was fitted by three peaks at 399.0, 400.8, and 404.9 eV. The major peak at 399.0 eV was ascribed to the sp^2 hybridized N atoms (C−N═C) contained in the s-triazine ring. The peak at 400.8 eV is attributed to the [N−$(C)_3$] containing bridging N atoms and (C−NH_2) containing terminal amino groups, and the peak at 404.9 eV belonged to the charging effect in triazine.[52,64] The relative peak intensity of the C 1S and N 1s XPS spectra corresponding to the N═C−N group decreased in ZnO/g-C_3N_4 compared to that in g-C_3N_4. These findings indicated that the ZnO doping partially broke the g-C_3N_4 containing aromatic ring structure.[63] In addition, the pathway of charge carrier movement in the composite photocatalyst may be predicted using the measurement of binding energy shift.[65,66] Hence, it could be inspected that the major peaks of high-resolution C 1s and N 1s of ZnO/g-C_3N_4 were shifted toward higher binding energies compared to those of g-C_3N_4. The result indicated that the electrons are transferred from g-C_3N_4 to ZnO, which reveals significant support for the electron transfer mechanism of the ZnO/g-C_3N_4 heterojunction.[67,68] As shown in Figure 2d, the high-resolution O 1s XPS spectra of ZnO/g-C_3N_4 was deconvoluted into three peaks. The main peak at 531.8 eV is associated with the O_2^{2-} in the wurtzite structure of ZnO.[69] The other two small peaks at 529.6 and 533.6 eV may be ascribed to the −OH groups in the adsorbed H_2O or −OH groups on the ZnO/g-C_3N_4 surface. On the contrary, the high-resolution O 1s XPS spectra of g-C_3N_4 exhibited only one peak with small intensity, which is attributed to the −OH groups in the adsorbed H_2O or −OH groups on the g-C_3N_4 surface.[70] In Figure 2e, the high-resolution Zn 2p XPS spectra of ZnO/g-C_3N_4 revealed two peaks at 1022.4 and 1045.5 eV corresponding to the binding energies of Zn $2p_{3/2}$ and Zn $2p_{1/2}$, and the peaks are separated by 23.1 eV. The observations are in good agreement with the reported binding energy of the high-resolution Zn 2p XPS spectra of the ZnO/g-C_3N_4 composite.[71,72] Moreover, as shown in the survey spectrum of the ZnO/g-C_3N_4, the Augur peaks of Zn LMM were detected, which indicate the existence of Zn−N bonds.[52]

DRS Analysis. The optical characteristics of photocatalysts have an influence on their photocatalytic ability. Thus, UV−vis DRS of the g-C_3N_4, ZnO, and ZnO/g-C_3N_4 composites were analyzed at room temperature in order to inspect their light absorption abilities. The UV−vis DRS data, as expressed by the Kubelka−Munk function of the samples, are shown in Figure 3a. The ZnO nanoparticles can only absorb UV light, with an absorption edge at around 390 nm.[46] The prepared g-C_3N_4 has an absorption edge at about 430 nm, including the visible region.[73] A slightly red-shifted absorption edge of the ZnO/g-C_3N_4 was observed compared to both g-C_3N_4 and ZnO. The small amount of N atoms in the s-triazine rings may be replaced by the O in the ZnO, which slightly influenced the electron distribution and increased the visible light absorption ability to a small extent.[46,53,70] The optical band gap of g-C_3N_4 and ZnO/g-C_3N_4 was determined by using the Tauc equation of indirect transition.[74]

$$\alpha h\nu = A(h\nu - E_g)^2 \quad (3)$$

Furthermore, the optical band gap of ZnO was determined by using the Tauc equation of direct transition.[74]

$$\alpha h\nu = A(h\nu - E_g)^{1/2} \quad (4)$$

where α is the absorption coefficient, $h\nu$ is the photoenergy, A is a constant, and E_g is the optical band gap. Hence, by plotting the value of $(\alpha h\nu)^{1/2}$ versus $h\nu$, the optical band gap of g-C_3N_4 and ZnO/g-C_3N_4 was determined, and by plotting the value of $(\alpha h\nu)^2$ versus $h\nu$, the optical band gap of ZnO was determined (Figure 3b). The optical band gaps of g-C_3N_4, ZnO, and ZnO/g-C_3N_4 are estimated to be 2.93, 3.20, and 2.81 eV, respectively.

PL Analysis. The decrease in the electron hole-pair recombination rate of photocatalysts has an influence on their photocatalytic activity. In order to investigate the relative electron hole-pair recombination rate of g-C_3N_4, ZnO, and ZnO/g-C_3N_4, PL analysis was carried out at an excitation wavelength of 340 nm. It was observed that the PL intensity of the composite decreased by a substantial amount compared to that of both g-C_3N_4 and ZnO (Figure 3c). The PL quenching specifies that the electron−hole pair recombination rate was suppressed and photogenerated charge separation was facilitated due to the synergic effect of ZnO and g-C_3N_4 in the composite.[53] Hence, the decrease in the electron hole-pair recombination rate indicated the enhanced photocatalytic activity of the prepared ZnO/g-C_3N_4 composite.

EIS Analysis. A lower charge transfer resistance of a photocatalyst denotes a better photocatalytic efficiency. In order to analyze the relative charge transfer resistance of g-C_3N_4 and ZnO/g-C_3N_4, EIS analysis was carried out. The charge transfer resistance is denoted by the curvature radius of the EIS graph. The reduction of resistance as well as the increment of charge transfer were indicated by the smaller curvature radius. As shown in Figure 3d, the EIS resultant Nyquist plot of ZnO/g-C_3N_4 showed a smaller curvature radius compared to the curvature radius of g-C_3N_4, which indicated the greater charge transfer separation of ZnO/g-C_3N_4 compared to that of bare g-C_3N_4.

Morphological Study. The morphologies of g-C_3N_4, ZnO, and ZnO/g-C_3N_4 were explored by using SEM and

https://doi.org/10.1021/acsomega.4c05679
ACS Omega 2024, 9, 45090−45103

TEM analysis (Figure 4). The SEM and TEM images of g-C_3N_4 show a sheet-like layered morphology of the particles

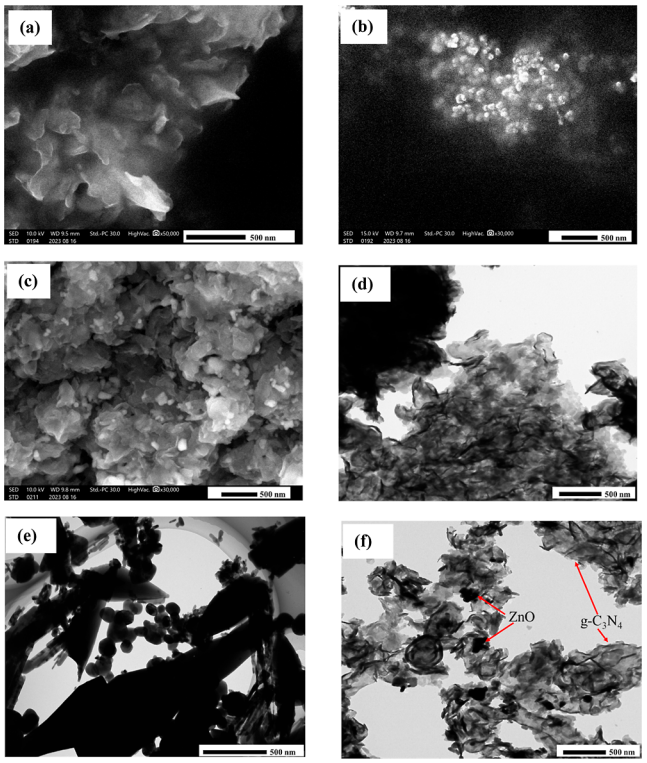

Figure 4. SEM images of (a) g-C_3N_4, (b) ZnO, and (c) ZnO/g-C_3N_4, and TEM images of (d) g-C_3N_4, (e) ZnO, and (f) ZnO/g-C_3N_4.

(Figure 4a,d). As shown in Figure 4b,e the semispherical particles of different sizes are observed in the SEM and TEM images of ZnO. The SEM and TEM images of the ZnO/g-C_3N_4 composites show that particles with different sizes and shapes corresponding to ZnO are well attached to the surface of sheet like layered g-C_3N_4 (Figure 4c,f). Hence, ZnO could be inserted and distributed to the surface of g-C_3N_4 after the thermal treatment.[30,32] Thus, the fabricated binary nanocomposite materials are expected to play a vital role in visible light-driven photocatalytic applications.

The elemental mapping of ZnO/g-C_3N_4 was investigated by EDS analysis. From Figure 5, it can be clearly seen that C, N, O, and Zn are dispersed on the surface of the composite. Furthermore, the ratio of relative color intensities for all elements is similar over all surfaces, as shown in Figure 5b–e, which indicates that the elements are homogeneously distributed. Hence, the morphological analysis confirms the formation and purity of the composite.

BET Surface Area and Pore Size Distribution Analysis. In order to determine the surface area and porous structure characteristics of the composite, measurements of N_2 adsorption–desorption isotherms and pore-size distributions of bare g-C_3N_4 and the ZnO/g-C_3N_4 composite were carried out. As shown in Figure 6, both g-C_3N_4 and ZnO/g-C_3N_4 displayed a typical type IV adsorption–desorption isotherm with H3 hysteresis loops. These indicated the existence of mesoporous material in the structure of g-C_3N_4 and ZnO/g-C_3N_4.[75] The specific surface areas, total pore volumes, and average pore sizes of g-C_3N_4 and ZnO/g-C_3N_4 are given in Table 1. It was observed that these values did not change

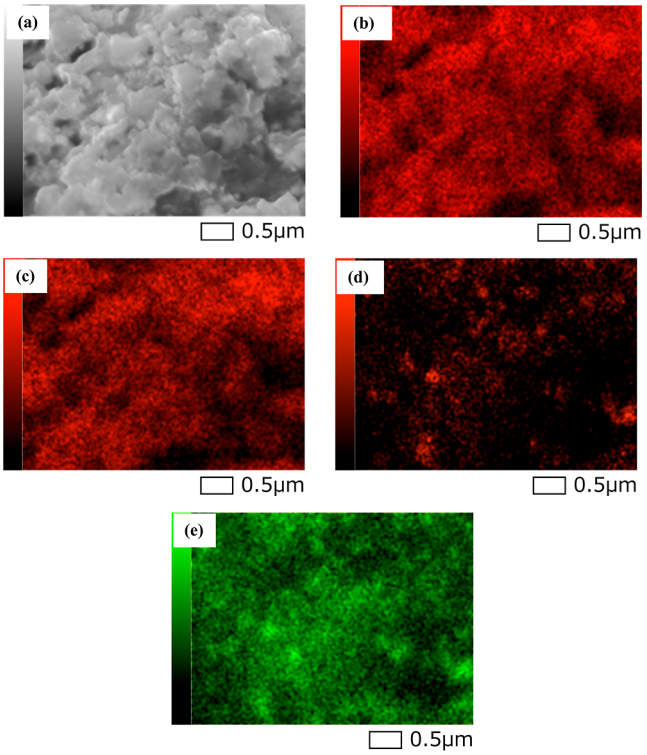

Figure 5. (a) SEM and EDS elemental mapping of (b) C, (c) N, (d) O, and (e) Zn of ZnO/g-C_3N_4.

significantly after the formation of the composite. The specific surface areas, total pore volumes, and average pore size values of ZnO/g-C_3N_4 are slightly smaller than those of the g-C_3N_4. Hence, the changes may not contribute to the enhanced photocatalytic efficiency of the composite.

Mott–Schottky Plot and Valence Band (VB)-XPS Analysis. In order to determine the flat-band potential (E_{FB}) as well as the conduction band potential (E_{CB}) of the ZnO/g-C_3N_4 composite, a Mott–Schottky plot has been constructed. As shown in Figure S3a, the positive slope of the plot indicates that the composite is an n-type semiconductor, and the major charge carriers in the composite are electrons. The E_{FB} value of ZnO/g-C_3N_4 was determined with respect to the abscissa axis and the intercept among the tangent lines of the plot. The E_{FB} value was estimated at −1.09 V (vs Ag/AgCl at pH 0), which can be converted to −0.48 V (vs normal hydrogen scale electrode (NHE) at pH 0) using the eq 5.[67]

$$E(\text{NHE at pH 0}) = E(\text{Ag/AgCl at pH 7}) + 0.196 + 0.059 \times 7 \quad (5)$$

According to the previous literature report, the position of the E_{CB} exist by is 0.1 eV upper than that of the E_{FB}.[76] Hence, the E_{CB} of the composite was estimated at −0.58 V (vs NHE at pH 0). The E_{VB} of the composite can be determined using the eq 6.

$$E_g = E_{VB} - E_{CB} \quad (6)$$

where the band gap of the composite (E_g) is 2.81 eV, which was determined by the Tauc plot as shown in Figure 3b. Thus, the calculated E_{VB} of the composite was 2.23 V (vs NHE at pH 0).

Moreover, the E_{VB} of the composite was calculated using VB-XPS analysis. As shown in Figure S3b, the VB edge of the

https://doi.org/10.1021/acsomega.4c05679
ACS Omega 2024, 9, 45090−45103

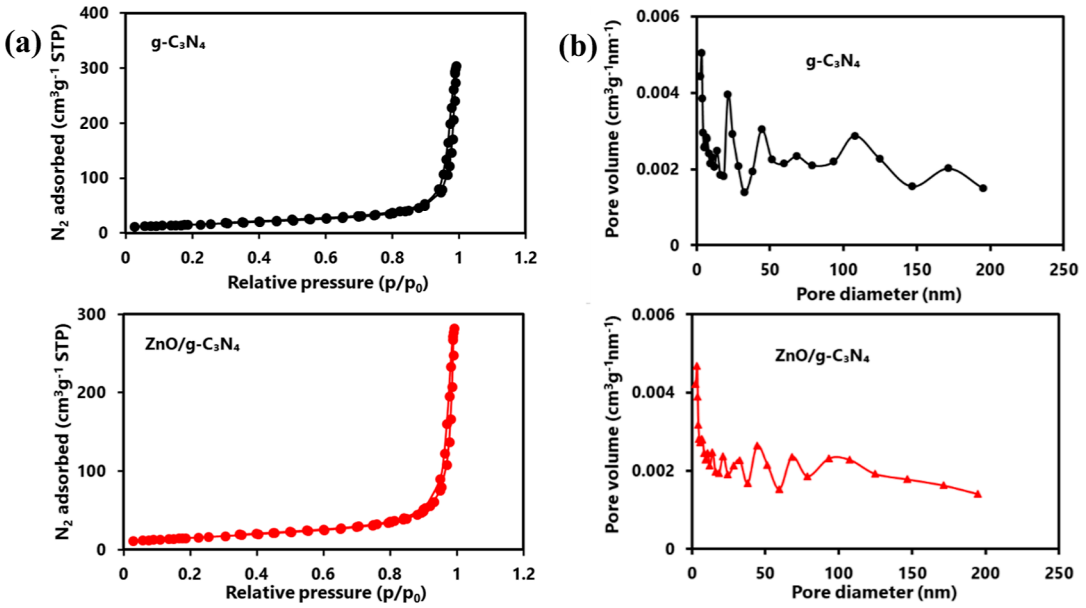

Figure 6. (a) N_2 adsorption−desorption isotherms, (b) pore size distribution curves of g-C_3N_4 and ZnO/g-C_3N_4.

Table 1. Surface Area, Pore Volume, and Pore Diameter of the g-C_3N_4 and ZnO/g-C_3N_4

photocatalyst	BET surface area (m^2/g)	total pore volume (cm^3/g)	average pore diameter (nm)
C_3N_4	55.67	0.44	31.88
ZnO/g-C_3N_4	53.67	0.40	30.32

ZnO/g-C_3N_4 was observed at about 1.93 eV. Hence, the VB position of the ZnO/g-C_3N_4 was corrected to the NHE scale using the following equation.[77]

$$E_{NHE}/V = \Phi_{WF} + \Phi_{sample} - 4.44 \quad (7)$$

where E_{NHE} is the E_{VB} of the composite at the NHE scale at pH 7.0, Φ_{WF} is the electron work function of the analyzer (4.33 eV), and Φ_{sample} is the VB edge of the ZnO/g-C_3N_4 (eV) in VB-XPS analysis. Hence, the corrected E_{VB} of ZnO/g-C_3N_4 is 1.82 V (vs NHE scale at pH 7.0). By addition of 0.413 V, the obtained E_{VB} of ZnO/g-C_3N_4 is corrected to be 2.23 V (vs NHE scale at pH 0). Hence, the result of VB-XPS is consistent with the result attained from the Mott−Schottky plot.

Photocatalytic Degradation of DCF. Figure 7 shows the photocatalytic degradation of DCF using ZnO/g-C_3N_4 composite and other corresponding catalysts at optimal condition. The photolysis reaction of DCF was also investigated. It was observed that the DCF was not degraded in the photolysis reaction, and g-C_3N_4 and ZnO showed negligible photocatalytic activity to degrade the DCF with visible light irradiation, while the physical mixture of ZnO and g-C_3N_4 at a 1:3 ratio showed moderate photocatalytic activity. Moreover, the ZnO/g-C_3N_4 exhibited excellent photocatalytic degradation ability for DCF. From Figure 7b, it was observed that the degradation processes followed the pseudo first order reaction kinetics equation (eq 2). It was observed that the rate constant of visible light-driven DCF degradation using the ZnO/g-C_3N_4 was 0.0541 min^{-1}, which was about 34 and 27

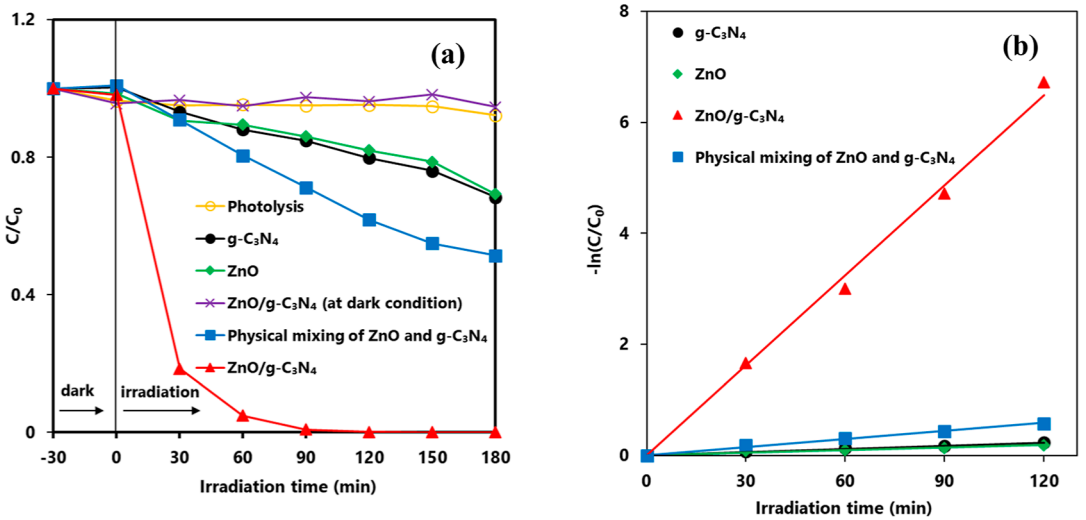

Figure 7. (a) Photocatalytic degradation of DCF using different catalyst with the irradiation of visible light and (b) the plot of $-\ln(C/C_0)$ versus irradiation time; DCF: 10 mg L^{-1} (30 mL), photocatalyst: 30 mg.

https://doi.org/10.1021/acsomega.4c05679
ACS Omega 2024, 9, 45090−45103

times higher than that attained with bare commercial ZnO and prepared g-C_3N_4, respectively, and 11 times higher than that attained with the physical mixture of ZnO and g-C_3N_4 (Table 2). The decrease in the electron hole-pair recombination rate

Table 2. Kinetic Parameters for Photocatalytic Degradation of DCF

photocatalyst	rate constant (min^{-1})	$T_{1/2}$ (min)	R^2
ZnO	0.0016	433.1	0.92
g-C_3N_4	0.0020	346.5	0.98
physical mixing of ZnO and g-C_3N_4	0.0049	141.4	0.99
ZnO/g-C_3N_4	0.0541	12.8	0.99

and the increment in charge transfer separation were responsible for the enhancement of the photocatalytic ability of the ZnO/g-C_3N_4 composite. The enhanced visible light response capacity with small amounts of the ZnO/g-C_3N_4 composite also affected its efficient photocatalytic capacity. However, textural properties such as specific surface areas, total pore volumes, and average pore sizes of the photocatalysts in this study did not control their photocatalytic efficacy.

Effect of ZnO Content. In order to determine the optimal mixing ratio of g-C_3N_4 and ZnO for fabricating the ZnO/g-C_3N_4 composite at photocatalytic degradation of DCF, the mixing ratio of g-C_3N_4 and ZnO was changed such that the total quantity was 200 mg. From Figure S4 and Table S1, it was found that the maximum degradation of DCF was observed using the composite fabricated from a 1:3 ratio of ZnO and g-C_3N_4. The photocatalytic degradation of DCF was improved with increasing amounts of g-C_3N_4 until the mentioned ratio, then decreased with further increasing g-C_3N_4 amounts. The synergistic effect of ZnO and g-C_3N_4 at this ratio could be responsible for improved photocatalytic degradation ability.[71]

Effect of Calcination Temperature. To understand the role of calcination temperature during the fabrication of the ZnO/g-C_3N_4 composite on the photocatalytic degradation of DCF, composites were prepared at different calcination temperatures, such as 350, 400, and 450 °C. The composite was also prepared without calcination. In every case, the other conditions for fabricating the composites were the same. As shown in Figure S5 and Table S2, it can be observed that the composite formed at 400 °C showed maximum photocatalytic activity compared to others. The composite formed without calcination could not show significant photocatalytic activity. The ZnO nanoparticles may be covered perfectly by g-C_3N_4, due to the lower degree of thermal polymerization of the g-C_3N_4 framework at 400 °C. The synergistic effect of ZnO and g-C_3N_4 at 400 °C as calcination temperature are attributed to the electron transfer from g-C_3N_4 to ZnO could be responsible for enhanced photocatalytic degradation efficiency. Thus, temperature plays an effective role in the formation of optimal composite. It means that the mixture of ZnO and g-C_3N_4 in a 1:3 ratio was calcined at 400 °C, which was the optimal condition for the composite fabrication.

Effect of Types of ZnO and g-C_3N_4. In order to investigate the effect of types of ZnO and g-C_3N_4 in the preparation of the composite on the photocatalytic degradation of DCF, commercially available ZnO was obtained from Sigma-Aldrich and Wako Chemicals, and two sets of ZnO were also prepared by calcination of zinc acetate and zinc nitrate at 550 °C for 2 h. Moreover, two sets of g-C_3N_4 were prepared by calcination of urea and melamine at 550 °C for 2 h. After that, eight sets of composites were prepared according to the procedure mentioned in the experimental section. It was observed that the composite of commercially obtained ZnO from Sigma-Aldrich and prepared g-C_3N_4 from calcination of urea showed superior photocatalytic DCF degradation ability compared to that of other composites (Figure S6 and Table S3).

Effect of Catalyst Dosage. In order to optimize the photocatalyst dosage for the degradation of DCF, the amount of ZnO/g-C_3N_4 composite was varied from 5 mg/30 mL to 50 mg/30 mL. It was observed that the degradation of DCF improved with rising the quantity of ZnO/g-C_3N_4 composite (Figure S7 and Table S4). The number of active sites could increase with an increasing amount of photocatalyst. But the increasing rate of degradation was slower, if the photocatalyst amount exceeded 30 mg/30 mL. An excess amount of ZnO/g-C_3N_4 may turbidize the reaction solution, hinder light

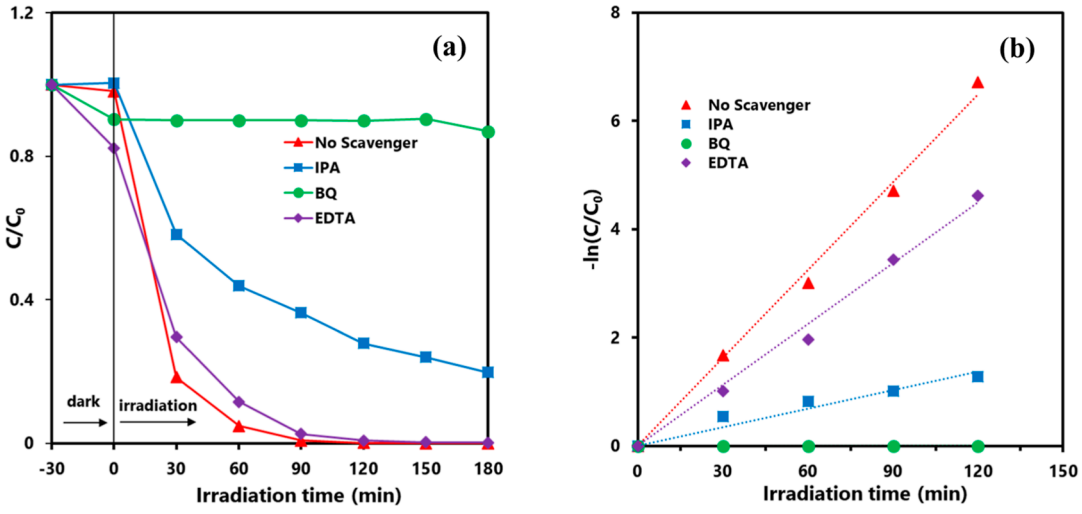

Figure 8. (a) Effect of scavenger on the photocatalytic degradation of DCF using ZnO/g-C_3N_4, and (b) the plot of -ln(C/C_0) versus irradiation time; DCF: 10 mg L^{-1} (30 mL), ZnO/g-C_3N_4: 30 mg.

https://doi.org/10.1021/acsomega.4c05679
ACS Omega 2024, 9, 45090−45103

penetration, saturate the number of active sites, and impact the increasing rate of degradation.[54,78] Hence, considering the degradation rate relative to the catalyst dosage and to minimize the use of excess amounts of photocatalyst, 30 mg/30 mL ZnO/g-C_3N_4 was selected as the optimal amount of photocatalyst for further study.

Effect of Initial Concentration of DCF. In order to inspect the effect of the initial concentration of DCF, the photocatalytic degradation of DCF using a 30 mg/30 mL ZnO/g-C_3N_4 composite has been studied, with the initial concentration of DCF varying from 5 to 50 mg L^{-1}. It was observed that the degradation rate of DCF decreased with increasing concentrations. Increasing the quantity of molecules attached to a fixed amount of the catalyst surface may prevent light absorption, and the probability of the creation of reactive species such as •OH and $•O_2^-$ would decrease on the surface of the catalyst. Thus, the photocatalytic degradation rate was decreased.[58] Furthermore, as shown in Figure S8 and Table S5, the degraded amount of DCF increased with increasing initial concentrations of DCF. Eventually, the degradation rate decreased and the degraded amount increased with increasing initial concentrations of DCF. Since very low concentrations and very high concentrations of DCF were insignificant for the practical application, 10 mg L^{-1} of DCF was selected as the initial concentration for the further experiment in this work.

Scavenger Role. It has been demonstrated that the photodegradation of organic pollutants involves several promising reactive species, including $•O_2^-$, •OH, and h^+. It was reported that BQ, IPA, and EDTA can function as efficient scavengers for $•O_2^-$, •OH, and h^+, respectively.[32] Hence, in order to fully comprehend the visible-light-induced photocatalytic degradation mechanism of DCF by ZnO/g-C_3N_4 composite, a series of radical scavenger experiments were carried out by using BQ, IPA, and EDTA as the scavengers of $•O_2^-$, •OH, and h^+, respectively. The obtained results are displayed in Figure 8 and Table 3. It can be seen that the photocatalytic degradation of DCF was almost inert in the presence of BQ, and the rate of degradation reaction was more than 1000 times slower than the rate without using any scavenger. On the other hand, IPA impacted the decrement of photocatalytic degradation of DCF significantly, and the degradation rate was about five times slower than the rate without using any scavenger. The results indicated that $•O_2^-$ plays a major reactive species in the photocatalytic degradation of DCF using fabricated ZnO/g-C_3N_4, while the •OH radical plays an important role. The EDTA also impacted the photocatalytic degradation of DCF slightly. Hence, the photogenerated h^+ may take part as a minor active radical on the degradation of DCF. The findings were in strong accordance with the scavenger function of the used ZnO/g-C_3N_4 on the photocatalytic degradation of methylene blue.[32]

Table 3. Impact of Scavenger on Kinetic Parameters for Photocatalytic Degradation of DCF Using ZnO/g-C_3N_4

scavenger	rate constant (min^{-1})	$T_{1/2}$ (min)	R^2
without	0.0541	12.8	0.99
IPA	0.0115	60.3	0.93
BQ	0.00005	13,860	0.55
EDTA	0.0375	18.5	0.99

Stability. Another crucial factor in determining whether a photocatalyst has a practical use in DCF degradation is its chemical durability upon application. Using five sequential reusability cycles of DCF degradation with visible light irradiation, the photostability of the ZnO/g-C_3N_4 composite was evaluated. It is evident, as shown in Figure S9, that the DCF degradation capacity of the composite considerably declined after five cycles of reuse. The chemisorption of DCF molecules or intermediate products of reaction on the more potent active sites of the photocatalyst, which persist after the saturation of the accessible sites for subsequent reactions, may be the cause of a little decrement in photocatalytic activity.[45] Hence, the result was attributed to the stability of the composite.

Mechanism. On the basis of the XPS result, it can be concluded that the electrons in the ZnO/g-C_3N_4 composite are spontaneously transferred from g-C_3N_4 to ZnO, and it is continued until their flat band potentials reach in equilibrium. After that, an internal electric field has been formed at the interface of the ZnO/g-C_3N_4 heterojunction (Figure S10). It can be assumed that a midlevel band appeared nearest to the CB of the ZnO in the composite, which is the CB of the composite −0.58 V (vs NHE at pH 0) (Figure 9). Considering the E_{CB} of ZnO and composite are equal, it can be said that The E_{CB} of ZnO was −0.58 V (vs NHE at pH 0). The E_{VB} of ZnO can be calculated to be 2.62 V (vs NHE at pH 0) using eq 6 and the value of the band gap of ZnO. As during the irradiation of visible light, electrons are transferred from the VB of g-C_3N_4 to CB of g-C_3N_4 and CB of ZnO, the E_{VB} of the composite can be assumed to be the E_{VB} of g-C_3N_4 2.23 V (vs NHE at pH 0). The E_{CB} of g-C_3N_4 can be calculated to −0.7 V (vs NHE at pH 0) using eq 6 and the value of the band gap of g-C_3N_4.

The photocatalytic degradation mechanism of DCF using the ZnO/g-C_3N_4 composite can be proposed by typical charge transfer and the interfacial charge transfer (IFCT) pathway. As shown in Figure 9, when g-C_3N_4 is subjected to visible light irradiation, photoelectrons and holes are generated on the CB and VB of the g-C_3N_4, respectively. Compared with ZnO, the E_{CB} in g-C_3N_4 has a greater negative value. In turn, this leads to the few photoelectrons in the CB of g-C_3N_4 being transferred to the CB of ZnO. Most of the photoelectrons are remained in the CB of g-C_3N_4 due to the formation of internal electric filed as mentioned before. Furthermore, photoelectrons can be transferred from the VB of g-C_3N_4 to the midlevel, as well as to the CB of the composite or the CB of ZnO, through the IFCT pathway. As a result, the e^-/h^+ pair recombination rate was suppressed. Hence, the separation efficiency of the photogenerated charges was enhanced. The photoelectrons in both CB of ZnO and CB of g-C_3N_4 were captured by the environmental oxygen and produced reactive radicals of $•O^{2-}$, as the CB potentials of both g-C_3N_4 and ZnO are significantly more negative compared to the standard $O_2/•O_2^-$ reduction potential (−0.28 V vs NHE at pH 0).[79] But the VB potential of g-C_3N_4 is less positive than the standard H_2O/•OH redox potential (2.80 V vs NHE at pH 0).[65] Hence, holes in g-C_3N_4 did not react with H_2O and could not create the reactive radical •OH. Noteworthy is the fact that the scavenger rule test indicates that not only the $•O_2^-$ radical but also the •OH radical plays important roles in the degradation of DCF in the present study. However, the •OH radical may be formed by the photochemical reaction of $•O^{2-}$, as shown in the eq 12.[74]

Moreover, the scavenger test also indicates that photogenerated h^+ takes part as a minor reactive species in the

https://doi.org/10.1021/acsomega.4c05679
ACS Omega 2024, 9, 45090−45103

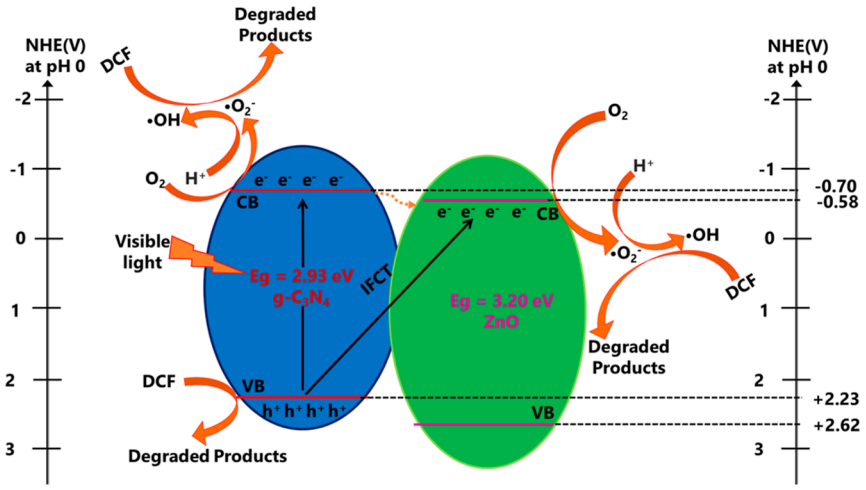

Figure 9. Mechanism of the photocatalytic degradation of DCF using ZnO/g-C_3N_4 composite.

photodegradation of DCF using the fabricated ZnO/g-C_3N_4 composite. Hence, a small amount of DCF may be degraded by the direct reaction of photogenerated holes in the VB of g-C_3N_4. The following equations represent the corresponding photocatalytic reactions of DCF degradation with the ZnO/g-C_3N_4 composite with visible light treatment.

$$\text{g-}C_3N_4 + \text{visible light} \rightarrow \text{g-}C_3N_4\ (e^- + h^+) \quad (8)$$

$$\text{g-}C_3N_4\ (e^-) + \text{ZnO} \rightarrow \text{ZnO}\ (e^-) + \text{g-}C_3N_4 \quad (9)$$

$$O_2 + \text{g-}C_3N_4\ (e^-) \rightarrow \text{ZnO} + \bullet O_2^- \quad (10)$$

$$O_2 + \text{ZnO}\ (e^-) \rightarrow \text{ZnO} + \bullet O_2^- \quad (11)$$

$$2H^+ + e^- + \bullet O_2^- \rightarrow H_2O_2 \rightarrow 2\bullet OH \quad (12)$$

$$\text{DCF} + \bullet O_2^-/\bullet OH \rightarrow \text{degraded products} \quad (13)$$

$$\text{DCF} + h^+ \rightarrow \text{degraded products} \quad (14)$$

CONCLUSIONS

In this study, the composite of commercially obtained ZnO (Sigma-Aldrich) and prepared g-C_3N_4 from the calcination of urea resulted in enhanced photocatalytic activity. Structural and morphological analysis revealed the successful formation of the composite, while PL and EIS analysis revealed the reduced recombination of photocharges in the fabricated composite. The photocatalytic degradation rate of DCF using ZnO/g-C_3N_4 composite was 27 times higher than that attained with pure g-C_3N_4 and 11 times higher than that attained with a physical mixture of ZnO and g-C_3N_4. Possible photocatalytic degradation mechanism and corresponding reactions have been proposed.

ASSOCIATED CONTENT

Supporting Information

The Supporting Information is available free of charge at https://pubs.acs.org/doi/10.1021/acsomega.4c05679.

Schematic diagram of ZnO/g-C_3N_4 synthesis, enlarged FTIR spectra, Mott−Schottky plot, VB-XPS plot, photocatalytic degradation of DCF using ZnO/g-C_3N_4 composite at different conditions, photocatalytic stability of the composite, and formation of internal electric field in the composite (PDF)

AUTHOR INFORMATION

Corresponding Authors

Mahmudul Hassan Suhag − *Department of Applied Chemistry, Graduate School of Engineering, Mie University, Tsu, Mie 514-8507, Japan; Department of Chemistry, University of Barishal, Barishal 8254, Bangladesh;* orcid.org/0000-0001-9214-3946; Email: suhag.che057@gmail.com

Satoshi Kaneco − *Department of Applied Chemistry, Graduate School of Engineering, Mie University, Tsu, Mie 514-8507, Japan;* orcid.org/0000-0002-6653-2312; Email: kaneco@chem.mie-u.ac.jp

Authors

Aklima Khatun − *Department of Applied Chemistry, Graduate School of Engineering, Mie University, Tsu, Mie 514-8507, Japan;* orcid.org/0000-0001-9899-8224

Ikki Tateishi − *Environmental Preservation Center, Mie University, Tsu, Mie 514-8507, Japan;* orcid.org/0000-0002-1484-5878

Mai Furukawa − *Department of Applied Chemistry, Graduate School of Engineering, Mie University, Tsu, Mie 514-8507, Japan*

Hideyuki Katsumata − *Department of Applied Chemistry, Graduate School of Engineering, Mie University, Tsu, Mie 514-8507, Japan;* orcid.org/0000-0002-4634-4998

Complete contact information is available at: https://pubs.acs.org/10.1021/acsomega.4c05679

Author Contributions

M.H.S.: conceptualization, methodology, data curation, formal analysis, investigation, writing- original draft, and writing—review and editing. A.K.: formal analysis, and writing—review and editing. I. T.: formal analysis, and writing—review and editing. M.F.: formal analysis, and writing—review and editing. H.K.: writing—review and editing. S.K.: writing—review and editing, and supervision.

Notes

The authors declare no competing financial interest.

https://doi.org/10.1021/acsomega.4c05679
ACS Omega 2024, 9, 45090−45103

■ ACKNOWLEDGMENTS

This research work was partially funded by the Grant-in-Aid for Scientific Research (B) 21H03642 from the Ministry of Education, Culture, Sports, Science, and Technology of Japan.

■ REFERENCES

(1) Zhang, W.; Zhou, L.; Shi, J.; Deng, H. Fabrication of Novel Visible-Light-Driven AgI/g-C_3N_4 Composites with Enhanced Visible-Light Photocatalytic Activity for Diclofenac Degradation. *J. Colloid Interface Sci.* **2017**, *496*, 167−176.

(2) Zhang, W.; Zhou, L.; Deng, H. Ag Modified g-C_3N_4 Composites with Enhanced Visible-Light Photocatalytic Activity for Diclofenac Degradation. *J. Mol. Catal. A Chem.* **2016**, *423*, 270−276.

(3) He, J.; Yang, J.; Jiang, F.; Liu, P.; Zhu, M. Photo-Assisted Peroxymonosulfate Activation via 2D/2D Heterostructure of Ti_3C_2/g-C_3N_4 for Degradation of Diclofenac. *Chemosphere* **2020**, *258*, 127339.

(4) Lara-Pérez, C.; Leyva, E.; Zermeño, B.; Osorio, I.; Montalvo, C.; Moctezuma, E. Photocatalytic Degradation of Diclofenac Sodium Salt: Adsorption and Reaction Kinetic Studies. *Environ. Earth Sci.* **2020**, *79* (11), 277.

(5) Tanveer, M.; Tezcanli, G.; Sadiq, M. T.; Kazmi, S. M.; Noshad, N.; Abbas, G.; Ali, A. Degradation of Diclofenac under Irradiation of UV Lamp and Solar Light Using ZnO Photo Catalyst. *Eng. Proc.* **2022**, *12* (1), 76.

(6) Gerbaldo, M. V.; Marchetti, S. G.; Mendoza, S. M.; Elias, V. R.; Mendieta, S. N.; Crivello, M. E. Photocatalytic Degradation of Sodium Diclofenac Using Spinel Ferrites: Kinetic Aspects. *Top. Catal.* **2022**, *65* (13−16), 1419−1426.

(7) Liu, W.; Li, Y.; Liu, F.; Jiang, W.; Zhang, D.; Liang, J. Visible-Light-Driven Photocatalytic Degradation of Diclofenac by Carbon Quantum Dots Modified Porous g-C_3N_4: Mechanisms, Degradation Pathway and DFT Calculation. *Water Res.* **2019**, *151*, 8−19.

(8) Lonappan, L.; Brar, S. K.; Das, R. K.; Verma, M.; Surampalli, R. Y. Diclofenac and Its Transformation Products: Environmental Occurrence and Toxicity - A Review. *Environ. Int.* **2016**, *96*, 127−138.

(9) Oaks, J. L.; Gilbert, M.; Virani, M. Z.; Watson, R. T.; Meteyer, C. U.; Rideout, B. A.; Shivaprasad, H. L.; Ahmed, S.; Chaudhry, M. J. I.; Arshad, M.; Mahmood, S.; Ali, A.; Khan, A. A. Diclofenac Residues as the Cause of Vulture Population Decline in Pakistan. *Nature* **2004**, *427* (6975), 630−633.

(10) Zhang, W.; Zhou, L.; Shi, J.; Deng, H. Synthesis of Ag_3PO_4/g-C_3N_4 Composite with Enhanced Photocatalytic Performance for the Photodegradation of Diclofenac under Visible Light Irradiation. *Catalysts* **2018**, *8* (2), 45.

(11) Malhotra, M.; Suresh, S.; Garg, A. Tea Waste Derived Activated Carbon for the Adsorption of Sodium Diclofenac from Wastewater: Adsorbent Characteristics, Adsorption Isotherms, Kinetics, and Thermodynamics. *Environ. Sci. Pollut. Res.* **2018**, *25* (32), 32210−32220.

(12) Chen, J.; Qian, Y.; Liu, H.; Huang, T. Oxidative Degradation of Diclofenac by Thermally Activated Persulfate: Implication for ISCO. *Environ. Sci. Pollut. Res.* **2016**, *23* (4), 3824−3833.

(13) Yang, W.; Wu, Y.; Zhang, L.; Jiang, J.; Feng, L. Removal of Five Selected Pharmaceuticals by Coagulation in the Presence of Dissolved Humic Acids and Kaolin. *Desalin. Water Treat.* **2015**, *54* (4−5), 1134−1140.

(14) Park, J.; Yamashita, N.; Tanaka, H. Membrane Fouling Control and Enhanced Removal of Pharmaceuticals and Personal Care Products by Coagulation-MBR. *Chemosphere* **2018**, *197*, 467−476.

(15) Ji, Z.; Liu, T.; Tian, H. Electrochemical Degradation of Diclofenac for Pharmaceutical Wastewater Treatment. *Int. J. Electrochem. Sci.* **2017**, *12* (8), 7807−7816.

(16) Chen, P.; Zhang, Q.; Su, Y.; Shen, L.; Wang, F.; Liu, H.; Liu, Y.; Cai, Z.; Lv, W.; Liu, G. Accelerated Photocatalytic Degradation of Diclofenac by a Novel CQDs/BiOCOOH Hybrid Material under Visible-Light Irradiation: Dechloridation, Detoxicity, and a New Superoxide Radical Model Study. *Chem. Eng. J.* **2018**, *332*, 737−748.

(17) Czech, B.; Buda, W. Multicomponent Nanocomposites for Elimination of Diclofenac in Water Based on an Amorphous TiO_2 Active in Various Light Sources. *J. Photochem. Photobiol. A Chem.* **2016**, *330*, 64−70.

(18) Shi, J. W.; Wang, Z.; He, C.; Wang, H.; Chen, J. W.; Fu, M. L.; Li, G.; Niu, C. CdS Quantum Dots Modified N-Doped Titania Plates for the Photocatalytic Mineralization of Diclofenac in Water under Visible Light Irradiation. *J. Mol. Catal. A Chem.* **2015**, *399*, 79−85.

(19) Kanakaraju, D.; Motti, C. A.; Glass, B. D.; Oelgemöller, M. Solar Photolysis versus TiO_2-Mediated Solar Photocatalysis: A Kinetic Study of the Degradation of Naproxen and Diclofenac in Various Water Matrices. *Environ. Sci. Pollut. Res.* **2016**, *23* (17), 17437−17448.

(20) Hama Aziz, K. H.; Miessner, H.; Mueller, S.; Kalass, D.; Moeller, D.; Khorshid, I.; Rashid, M. A. M. Degradation of Pharmaceutical Diclofenac and Ibuprofen in Aqueous Solution, a Direct Comparison of Ozonation, Photocatalysis, and Non-Thermal Plasma. *Chem. Eng. J.* **2017**, *313*, 1033−1041.

(21) Das, L.; Barodia, S. K.; Sengupta, S.; Basu, J. K. Aqueous Degradation Kinetics of Pharmaceutical Drug Diclofenac by Photocatalysis Using Nanostructured Titania−zirconia Composite Catalyst. *Int. J. Environ. Sci. Technol.* **2015**, *12* (1), 317−326.

(22) Moreira, N. F. F.; Orge, C. A.; Ribeiro, A. R.; Faria, J. L.; Nunes, O. C.; Pereira, M. F. R.; Silva, A. M. T. Fast Mineralization and Detoxification of Amoxicillin and Diclofenac by Photocatalytic Ozonation and Application to an Urban Wastewater. *Water Res.* **2015**, *87*, 87−96.

(23) Moctezuma, E.; Leyva, E.; Lara-Pérez, C.; Noriega, S.; Martínez-Richa, A. TiO_2 Photocatalytic Degradation of Diclofenac: Intermediates and Total Reaction Mechanism. *Top. Catal.* **2020**, *63* (5−6), 601−615.

(24) Jiménez-Salcedo, M.; Monge, M.; Tena, M. T. The Photocatalytic Degradation of Sodium Diclofenac in Different Water Matrices Using g-C_3N_4 Nanosheets: A Study of the Intermediate by-Products and Mechanism. *J. Environ. Chem. Eng.* **2021**, *9* (5), 105827.

(25) Du, X.; Yi, X.; Wang, P.; Deng, J.; Wang, C. C. Enhanced Photocatalytic Cr(VI) Reduction and Diclofenac Sodium Degradation under Simulated Sunlight Irradiation over MIL-100(Fe)/g-C_3N_4 Heterojunctions. *Chin. J. Catal.* **2019**, *40* (1), 70−79.

(26) Ravichandran, K.; Kalpana, K.; Ibrahim, M. M.; Seelan, K. S. Effect of Source Material of g-C_3N_4 on the Photocatalytic Activity of ZnO/g-C_3N_4 thin Film Coated on Stainless Steel Mesh Substrate. *Mater. Today: Proc.* **2019**, *48*, 207−215.

(27) Oliveros, A. N.; Pimentel, J. A. I.; de Luna, M. D. G.; Garcia-Segura, S.; Abarca, R. R. M.; Doong, R. A. Visible-Light Photocatalytic Diclofenac Removal by Tunable Vanadium Pentoxide/boron-Doped Graphitic Carbon Nitride Composite. *Chem. Eng. J.* **2021**, *403*, 126213.

(28) Hu, Z.; Cai, X.; Wang, Z.; Li, S.; Wang, Z.; Xie, X. Construction of Carbon-Doped Supramolecule-Based g-C_3N_4/TiO_2 Composites for Removal of Diclofenac and Carbamazepine: A Comparative Study of Operating Parameters, Mechanisms, Degradation Pathways. *J. Hazard. Mater.* **2019**, *380*, 120812.

(29) Shao, H.; Zhao, X.; Wang, Y.; Mao, R.; Wang, Y.; Qiao, M.; Zhao, S.; Zhu, Y. Synergetic Activation of Peroxymonosulfate by Co_3O_4 Modified g-C_3N_4 for Enhanced Degradation of Diclofenac Sodium under Visible Light Irradiation. *Appl. Catal. B Environ.* **2017**, *218*, 810−818.

(30) Alharthi, F. A.; Ali Alghamdi, A.; Alanazi, H. S.; Alsyahi, A. A.; Ahmad, N. Photocatalytic Degradation of the Light Sensitive Organic Dyes: Methylene Blue and Rose Bengal by Using Urea Derived g-C_3N_4/ZnO Nanocomposites. *Catalysts* **2020**, *10* (12), 1457.

(31) Prasad Adhikari, S.; Raj Pant, H.; Joo Kim, H.; Hee Park, C.; Sang Kim, C. Deposition of ZnO Flowers on the Surface of g-C_3N_4 Sheets via Hydrothermal Process. *Ceram. Int.* **2015**, *41* (10), 12923−12929.

(32) Gayathri, M.; Sakar, M.; Satheeshkumar, E.; Sundaravadivel, E. Insights into the Mechanism of ZnO/g-C_3N_4 Nanocomposites toward

https://doi.org/10.1021/acsomega.4c05679
ACS Omega 2024, 9, 45090−45103

Photocatalytic Degradation of Multiple Organic Dyes. *J. Mater. Sci. Mater. Electron.* **2022**, *33* (12), 9347−9357.
(33) Kumar, S. G.; Kavitha, R.; Manjunatha, C. Review and Perspective on Rational Design and Interface Engineering of g-C_3N_4/ZnO: From Type-II to Step-Scheme Heterojunctions for Photocatalytic Applications. *Energy Fuels* **2023**, *37* (19), 14421−14472.
(34) Qin, J.; Yang, C.; Cao, M.; Zhang, X.; Rajendran, S.; Limpanart, S.; Ma, M.; Liu, R. Two-Dimensional Porous Sheet-like Carbon-Doped ZnO/g-C_3N_4 nanocomposite with High Visible-Light Photocatalytic Performance. *Mater. Lett.* **2017**, *189*, 156−159.
(35) Liu, W.; Wang, M.; Xu, C.; Chen, S.; Fu, X. Significantly Enhanced Visible-Light Photocatalytic Activity of g-C_3N_4 via ZnO Modification and the Mechanism Study. *J. Mol. Catal. A Chem.* **2013**, *368*−*369*, 9−15.
(36) Park, T. J.; Pawar, R. C.; Kang, S.; Lee, C. S. Ultra-Thin Coating of g-C_3N_4 on an Aligned ZnO Nanorod Film for Rapid Charge Separation and Improved Photodegradation Performance. *RSC Adv.* **2016**, *6* (92), 89944−89952.
(37) Wang, J.; Yang, Z.; Gao, X.; Yao, W.; Wei, W.; Chen, X.; Zong, R.; Zhu, Y. Core-Shell g-C_3N_4@ZnO Composites as Photoanodes with Double Synergistic Effects for Enhanced Visible-Light Photoelectrocatalytic Activities. *Appl. Catal. B Environ.* **2017**, *217*, 169−180.
(38) Liu, B.; Bie, C.; Zhang, Y.; Wang, L.; Li, Y.; Yu, J. Hierarchically Porous ZnO/g-C_3N_4 s-Scheme Heterojunction Photocatalyst for Efficient H_2O_2 production. *Langmuir* **2021**, *37* (48), 14114−14124.
(39) Chen, C.; Jin, J.; Chen, S.; Wang, T.; Xiao, J.; Peng, T. In-Situ Growth of Ultrafine ZnO on g-C_3N_4 Layer for Highly Active and Selective CO_2 Photoreduction to CH_4 under Visible Light. *Mater. Res. Bull.* **2021**, *137*, 111177.
(40) de Jesus Martins, N.; Gomes, I. C. H.; da Silva, G. T. S. T.; Torres, J. A.; Avansi, W.; Ribeiro, C.; Malagutti, A. R.; Mourão, H. A. J. L. Facile Preparation of ZnO: g-C_3N_4 Heterostructures and Their Application in Amiloride Photodegradation and CO_2 Photoreduction. *J. Alloys Compd.* **2021**, *856*, 156798.
(41) Liu, J.; Yan, X. T.; Qin, X. S.; Wu, S. J.; Zhao, H.; Yu, W. B.; Chen, L. H.; Li, Y.; Su, B. L. Light-Assisted Preparation of Heterostructured g-C_3N_4/ZnO Nanorods Arrays for Enhanced Photocatalytic Hydrogen Performance. *Catal. Today* **2020**, *355*, 932−936.
(42) Khatun, A.; Suhag, M. H.; Tateishi, I.; Furukawa, M.; Katsumata, H.; Kaneco, S. Facile Synthesis of ZnO/g-C_3N_4 with Enhanced Photocatalytic Performance for the Reduction of Cr(VI) in Presence of EDTA Under Visible Light Irradiation. *Int. J. Environ. Res.* **2023**, *17* (2), 32.
(43) Paul, D. R.; Gautam, S.; Panchal, P.; Nehra, S. P.; Choudhary, P.; Sharma, A. ZnO-Modified g-C_3N_4: A Potential Photocatalyst for Environmental Application. *ACS Omega* **2020**, *5* (8), 3828−3838.
(44) Nemiwal, M.; Zhang, T. C.; Kumar, D. Recent Progress in g-C_3N_4, TiO_2 and ZnO Based Photocatalysts for Dye Degradation: Strategies to Improve Photocatalytic Activity. *Sci. Total Environ.* **2021**, *767*, 144896.
(45) Pérez-Molina, Á.; Pastrana-Martínez, L. M.; Pérez-Poyatos, L. T.; Morales-Torres, S.; Maldonado-Hódar, F. J. One-Pot Thermal Synthesis of g-C_3N_4/ZnO Composites for the Degradation of 5-Fluoruracil Cytostatic Drug under UV-LED Irradiation. *Nanomaterials* **2022**, *12* (3), 340.
(46) Ismael, M. The Photocatalytic Performance of the ZnO/g-C_3N_4 Composite Photocatalyst toward Degradation of Organic Pollutants and Its Inactivity toward Hydrogen Evolution: The Influence of Light Irradiation and Charge Transfer. *Chem. Phys. Lett.* **2020**, *739*, 136992.
(47) Meena, P. L.; Poswal, K.; Surela, A. K.; Saini, J. K. Synthesis of g-C_3N_4/ZnO Nanostructures via Mechano-Thermal Method for Photocatalytic Degradation of Methylene Blue Dye. *Int. J. Environ. Sci. Technol.* **2024**, *21*..
(48) Girish, Y. R.; Udayabhanu; Byrappa, N. M.; Alnaggar, G.; Hezam, A.; Nagaraju, G.; Pramoda, K.; Byrappa, K. Rapid and Facile Synthesis of Z-Scheme ZnO/g-C_3N_4 Heterostructure as Efficient Visible Light-Driven Photocatalysts for Dye Degradation and Hydrogen Evolution Reaction. *J. Hazard. Mater. Adv.* **2023**, *9*, 100230.
(49) Pham, T. H.; Tran, M. H.; Chu, T. T. H.; Myung, Y.; Jung, S. H.; Mapari, M. G.; Taeyoung, K. Enhanced Photodegradation of Tetracycline in Wastewater and Conversion of CO_2 by Solar Light Assisted ZnO/g-C_3N_4. *Environ. Res.* **2023**, *217*, 114825.
(50) Hosseini-Hosseinabad, S. M.; Minaeian, S.; Tavakoli, A.; Sabaei, M.; Yousefi Zoshk, M.; Laripour, R.; Ramezani, S.; Hoseini, M.; Chamanara, M. Development of g-C_3N_4/ZnO Nanocomposite as a Novel, Highly Effective and Durable Photocatalytic Antibacterial Coating for Cotton Fabric. *Ceram. Int.* **2023**, *49* (8), 12274−12284.
(51) Teye, G. K.; Huang, J.; Li, Y.; Li, K.; Chen, L.; Darkwah, W. K. Photocatalytic Degradation of Sulfamethoxazole, Nitenpyram and Tetracycline by Composites of Core Shell g-C_3N_4@ZnO, and ZnO Defects in Aqueous Phase. *Nanomaterials* **2021**, *11* (10), 2609.
(52) Jingyu, H.; Ran, Y.; Zhaohui, L.; Yuanqiang, S.; Lingbo, Q.; Nti Kani, A.; Kani, A. N. In-Situ Growth of ZnO Globular on g-C_3N_4 to Fabrication Binary Heterojunctions and Their Photocatalytic Degradation Activity on Tetracyclines. *Solid State Sci.* **2019**, *92*, 60−67.
(53) Sun, Q.; Sun, Y.; Zhou, M.; Cheng, H.; Chen, H.; Dorus, B.; Lu, M.; Le, T. A 2D/3D g-C_3N_4/ZnO Heterojunction Enhanced Visible-Light Driven Photocatalytic Activity for Sulfonamides Degradation. *Ceram. Int.* **2022**, *48* (5), 7283−7290.
(54) Garg, R.; Gupta, R.; Bansal, A. Synthesis of g-C_3N_4/ZnO Nanocomposite for Photocatalytic Degradation of a Refractory Organic Endocrine Disrupter. *Mater. Today Proc.* **2021**, *44*, 855−859.
(55) Suhag, M. H.; Khatun, A.; Tateishi, I.; Furukawa, M.; Katsumata, H.; Kaneco, S. One-Step Fabrication of the ZnO/g-C_3N_4 Composite for Visible Light-Responsive Photocatalytic Degradation of Bisphenol E in Aqueous Solution. *ACS Omega* **2023**, *8* (13), 11824−11836.
(56) Sun, J.-X.; Yuan, Y.-P.; Qiu, L.-G.; Jiang, X.; Xie, A.-J.; Shen, Y.-H.; Zhu, J.-F. Fabrication of Composite Photocatalyst g-C_3N_4-ZnO and Enhancement of Photocatalytic Activity under Visible Light. *Dalt. Trans.* **2012**, *41* (22), 6756−6763.
(57) Zhu, Y.-P.; Li, M.; Liu, Y.-L.; Ren, T.-Z.; Yuan, Z.-Y. Carbon-Doped ZnO Hybridized Homogeneously with Graphitic Carbon Nitride Nanocomposites for Photocatalysis. *J. Phys. Chem. C* **2014**, *118* (20), 10963−10971.
(58) Kumar, K. V. A.; Vinodkumar, T.; Selvaraj, M.; Suryakala, D.; Subrahmanyam, C. Visible Light-Induced Catalytic Abatement of 4-Nitrophenol and Rhodamine B Using ZnO/g-C_3N_4 Catalyst. *J. Chem. Sci.* **2021**, *133* (2), 41.
(59) Sharifalhoseini, Z.; Entezari, M. H.; Shahidi, M. Sonication Affects the Quantity and the Morphology of ZnO Nanostructures Synthesized on the Mild Steel and Changes the Corrosion Protection of the Surface. *Ultrason. Sonochem.* **2018**, *41*, 492−502.
(60) Kumaresan, N.; Sinthiya, M. M. A.; Sarathbavan, M.; Ramamurthi, K.; Sethuraman, K.; Babu, R. R. Synergetic Effect of g-C_3N_4/ZnO Binary Nanocomposites Heterojunction on Improving Charge Carrier Separation through 2D/1D Nanostructures for Effective Photocatalytic Activity under the Sunlight Irradiation. *Sep. Purif. Technol.* **2020**, *244*, 116356.
(61) Vu, M.-H.; Sakar, M.; Nguyen, C.-C.; Do, T.-O. Chemically Bonded Ni Cocatalyst onto the S Doped g-C_3N_4 Nanosheets and Their Synergistic Enhancement in H_2 Production under Sunlight Irradiation. *ACS Sustain. Chem. Eng.* **2018**, *6* (3), 4194−4203.
(62) Li, L.; Sun, S.-Q.; Wang, Y.-X.; Wang, C.-Y. Facile Synthesis of ZnO/g-C_3N_4 Composites with Honeycomb-like Structure by H_2 Bubble Templates and Their Enhanced Visible Light Photocatalytic Performance. *J. Photochem. Photobiol. A Chem.* **2018**, *355*, 16−24.
(63) Yue, B.; Li, Q.; Iwai, H.; Kako, T.; Ye, J. Hydrogen Production Using Zinc-Doped Carbon Nitride Catalyst Irradiated with Visible Light. *Sci. Technol. Adv. Mater.* **2011**, *12* (3), 034401.
(64) Suhag, M. H.; Katsumata, H.; Tateishi, I.; Furukawa, M.; Kaneco, S. Black Phosphorus-Doped Graphitic Carbon Nitride with Aromatic Benzene Rings for Efficient Photocatalytic Hydrogen Production. *Langmuir* **2023**, *39* (37), 13121−13131.

https://doi.org/10.1021/acsomega.4c05679
ACS Omega 2024, 9, 45090−45103

(65) Xu, Q.; Zhang, L.; Cheng, B.; Fan, J.; Yu, J. S-Scheme Heterojunction Photocatalyst. *Chem.* **2020**, *6* (7), 1543−1559.
(66) Wang, L.; Tan, H.; Zhang, L.; Cheng, B.; Yu, J. In-Situ Growth of Few-Layer Graphene on ZnO with Intimate Interfacial Contact for Enhanced Photocatalytic CO_2 Reduction Activity. *Chem. Eng. J.* **2021**, *411*, 128501.
(67) Huang, W.; Li, Z.; Wu, C.; Zhang, H.; Sun, J.; Li, Q. Delaminating Ti_3C_2 MXene by Blossom of $ZnIn_2S_4$ Microflowers for Noble-Metal-Free Photocatalytic Hydrogen Production. *J. Mater. Sci. Technol.* **2022**, *120*, 89−98.
(68) Bai, P.; Wang, P.; Wu, Y.; Pang, X.; Song, M.; Du, C.; Su, Y. Junction of $Zn_mIn_2S_{3+m}$ and Bismuth Vanadate as Z-Scheme Photocatalyst for Enhanced Hydrogen Evolution Activity: The Role of Interfacial Interactions. *J. Colloid Interface Sci.* **2022**, *628*, 488−499.
(69) Kotsis, K.; Staemmler, V. Ab Initio Calculations of the O1s XPS Spectra of ZnO and Zn Oxo Compounds. *Phys. Chem. Chem. Phys.* **2006**, *8* (13), 1490.
(70) Zhong, Q.; Lan, H.; Zhang, M.; Zhu, H.; Bu, M. Preparation of Heterostructure g-C_3N_4/ZnO Nanorods for High Photocatalytic Activity on Different Pollutants (MB, RhB, Cr(VI) and Eosin). *Ceram. Int.* **2020**, *46* (8), 12192−12199.
(71) Xing, H.; Ma, H.; Fu, Y.; Xue, M.; Zhang, X.; Dong, X.; Zhang, X. Preparation of g-C_3N_4/ZnO Composites and Their Enhanced Photocatalytic Activity. *Mater. Technol.* **2015**, *30* (2), 122−127.
(72) Das, J.; Pradhan, S. K.; Sahu, D. R.; Mishra, D. K.; Sarangi, S. N.; Nayak, B. B.; Verma, S.; Roul, B. K. Micro-Raman and XPS Studies of Pure ZnO Ceramics. *Phys. B Condens. Matter* **2010**, *405* (10), 2492−2497.
(73) Islam, J. B.; Islam, M. R.; Furukawa, M.; Tateishi, I.; Katsumata, H.; Kaneco, S. Ag-Modified g-C_3N_4 with Enhanced Activity for the Photocatalytic Reduction of Hexavalent Chromium in the Presence of EDTA under Ultraviolet Irradiation. *Environ. Technol.* **2023**, *44* (23), 3627−3640.
(74) Zhang, Z.; Sun, Y.; Wang, Y.; Yang, Y.; Wang, P.; Shi, L.; Feng, L.; Fang, S.; Liu, Q.; Ma, L.; Peng, S.; Wang, T. Synthesis and Photocatalytic Activity of g-C_3N_4/ZnO Composite Microspheres under Visible Light Exposure. *Ceram. Int.* **2022**, *48* (3), 3293−3302.
(75) Yang, P.; Wang, J.; Yue, G.; Yang, R.; Zhao, P.; Yang, L.; Zhao, X.; Astruc, D. Constructing Mesoporous g-C_3N_4/ZnO Nanosheets Catalyst for Enhanced Visible-Light Driven Photocatalytic Activity. *J. Photochem. Photobiol. A Chem.* **2020**, *388*, 112169.
(76) Jiang, R.; Lu, G.; Liu, J.; Wu, D.; Yan, Z.; Wang, Y. Incorporation of π-Conjugated Molecules as Electron Donors in g-C_3N_4 Enhances Photocatalytic H_2-Production. *Renewable Energy* **2021**, *164*, 531−540.
(77) Katsumata, H.; Islam Molla, M. A.; Islam, J. B.; Tateishi, I.; Furukawa, M.; Kaneco, S. Dual Z-Scheme Heterojunction g-C_3N_4/Ag_3PO_4/AgBr Photocatalyst with Enhanced Visible-Light Photocatalytic Activity. *Ceram. Int.* **2022**, *48* (15), 21898−21905.
(78) Paul, D. R.; Sharma, R.; Nehra, S. P.; Sharma, A. Effect of Calcination Temperature, pH and Catalyst Loading on Photodegradation Efficiency of Urea Derived Graphitic Carbon Nitride towards Methylene Blue Dye Solution. *RSC Adv.* **2019**, *9* (27), 15381−15391.
(79) Okunaka, S.; Kameshige, H.; Oozu, S.; Yang, Y.; Miyauchi, M.; Tokudome, H. Synthetic Strategies of $BiVO_4$ for Efficient Visible-Light-Induced Photocatalytic Oxidation Reactions: Activation via Nanoparticulation and Surface Modification. *J. Ceram. Soc. Japan* **2023**, *131* (7), 195−201.

https://doi.org/10.1021/acsomega.4c05679
ACS Omega 2024, 9, 45090−45103